Impact of Annealing Thin Films $In(OH)_xS_y$ Growth By Solution Technique

Cliff Orori Mosiori [1], Robert Magare [1], Mathew Munji [2]

[1] *Technical University of Mombasa*
P. O. Box 90420-80100, Mombasa, Kenya

[2] *Kenyatta University*
P. O. Box 43844–00100, Nairobi, Kenya

DOI: 10.22178/pos.24-3

LCC Subject Category: TP155-156

Received 12.06.2017
Accepted 10.07.2017
Published online 14.07.2017

Corresponding Author:
Mosiori Cliff Orori,
corori@tum.ac.ke

© 2017 The Authors. This article is licensed under a Creative Commons Attribution 4.0 License

Abstract. Indium Hydroxy Sulphide has demonstrated abundance in resources, low prices, nontoxic characteristics, radiation resistance, high temperature resistance, and chemical stability, and therefore it has become an extremely important photoelectric, photovoltaic, and light sensing thin film material. Some treatment on this material include thermal annealing which is a process used for intrinsic stress liberation, structural improving, and surface roughness to control its electro-optical properties. In a qualitative way, annealing modifies surface morphology, intrinsic parameters, and electron mobility with temperature and time. In this work, an explanation on the surface modification of $In(OH)_xS_y$ thin films when subjected to an annealing process is discussed. Both electrical and optical effects caused by annealing were carried out and characterizations were performed at different annealing temperatures in nitrogen in the temperature range 373–573 K. Using optical measurements data and simulated data, Scout software was employed and the results showed that increasing annealing temperature causes a slight decrease in transmittance with a consequence of modifying the energy band gaps values between 2.79–3.32 eV. It was concluded that annealing influence optical transmittance and resistance of the film make the thin films potential for photovoltaic, and light sensing applications.

Keywords: annealing; energy band gaps; recrystallization; optical effect; passivation; stoichiometry.

Introduction

Indium sulphide is a promising candidate for optoelectronic, photovoltaic, and many other technological applications due to its stability, wide band gap, and photoconductivity [21]. The optical band gap value reported for indium sulphide thin films lies in range 2.0–2.4 eV depending on the physical or chemical process deposition [2]. One possibility to induce anomalous broadening of the optical band gap is to substitute some sulphur with oxygen in order to synthesize a homogeneous $In_2S_{3-3x}O_{3x}$ [14]. Another possibility of a buffer containing hydroxides or oxides and hydroxides is by use of *CBD* for sulphides, since the composition of a buffer layer often depends on the deposition method and the preparation condition [9]. According to the research done on the electronic engineering of solid-state DSSC, passivation of interface recombination can be of fundamental importance in systems like ETA-solar cells [6] and $In(OH)_xS_y$ is one of the proposed buffer layers [18]. The $In(OH)_xS_y$ layers have been deposited by a wet CBD and has proved to be a good buffer for TiO_2 solar cells with its band gap energy varying in the range 2.4–3.4 eV depending on stoichiometry of $In(OH)_xS_y$ [14, 24]. The dark I-V characteristics obtained confirm that $In(OH)_xS_y$ coating was good and free of pin holes that can lead to shorting of the current. Consequently, after annealing the films at 300 °C for 30 minutes, the material changes from amorphous state to crystalline state and also becomes slightly rich in In_2S_3 content [24, 20]. The buffer film can minimize the

electron-hole pair recombination and the capability of the n-type semiconductor when infiltrated with the *p*-type absorber [25]. The dark I-V characteristics of $In(OH)_xS_y$ coating deposited by CBD confirm that it is appropriate for PV cells and does not have porosity which can give rise to shunting problems. In general, the performance of the solar cell under illumination for open circuit voltage and short circuit current density have been found to be 0.27 V and 11.7 mA/cm^2, respectively. The fill factor of about 0.32 with a conversion efficiency of 1.01 % V for the solar cell have also been realised [18]. The dependency of E_g on the *pH* value of the solution is most probably due to changes in the stoichiometry [23] of $In(OH)_xS_y$.

Thermal annealing. Annealing refers to a semiconductor manufacturing process which heats silicon wafers to high temperatures on a timescale of several seconds or less but during cooling, temperatures must be brought down slowly to prevent dislocations and wafer breakage due to thermal shock [16]. This process is used for a wide variety of applications in semiconductor manufacturing including dopant activation, thermal oxidation, metal re-flow, and chemical vapor deposition. It consists of heating a single wafer or thin film at a time in order to affect its electrical properties. Unique heat treatments are designed for different effects. Wafers or thin films can be heated in order to activate dopants, change film-to-film or film-to-wafer substrate interface [7], densify deposited films, change states of grown films, repair damage from ion implantation [4], move dopants or drive dopants from one film into another or from a film into the wafer substrate. Post annealing can also be performed. This treatment is an important technique which helps to enhance thin film properties by changing their microstructure and phase orientation. Annealing thin films have different consequences depending on the nature of the thin film. Annealing may relief strain due to lattice mismatch and hence modify its surface morphology [19]. As a rule of thumb, annealing at 1/3 of the melting temperature of the bulk material, in principle improves its surface roughness. Annealing can also favor the formation of certain specific structural phases and may equally trigger possible diffusion processes. This is because annealing strongly depends on the interaction potentials of the film and the type of substrate materials. If the interaction of films and substrate atoms is weak, heating will promote the formation of clusters or islands of the film material. If the interaction is strong, a smoothing of the film is possible. However, annealing at very higher temperature may have detrimental effects since it may disturb the interface with the substrate.

Methodology

Materials and Reagents. The following reagents were purchased from sigma Aldrich and were used without further purification: Indium (III) Chloride 99 %; Hydrochloric Acid 79 %; Thio-Acetamide 99.8 %; and De-Ionized water. Other chemical and laboratory requirements were obtained from the University of Nairobi, Material Science laboratories as required.

Experimental Procedures. Chemical Bath Technique (CBD) was used to grow Indium Hydroxy Sulphide thin films. After thorough cleaning the glass substrate, $In(OH)_xS_y$ was coating on them using chemical bath deposition technique at 70 °C for about 90 minutes from aqueous solution containing 5 ml Indium (III) Chloride (0.009 M), 2.5 ml Hydrochloric Acid (0.005 M), 6 ml Thio-Acetamide (0.6 M), *HCl* (0.005 M) and 26.5 ml De-Ionized water according to [1]. The growth process took about 25 minutes, at a constant temperature of 70 ± 1 °C as illustrated in Figure 1.

Figure 1 – Setup for chemical bath deposition used in depositing $In(OH)_xS_y$

All conditions maintained by [13] were followed. After every deposition the sample was gently rinsed in double distilled water before allowed to

dry and then kept in desiccators as reflected by [11].

Characterization. A spectrophotometer was to obtain reflectance and transmittance measurements in the spectral range of 50–2500 nm while electrical resistivity was measured by using the four point probe interfaced with the Keithley 2400 source meter. The *In(OH)$_x$S$_y$* films were finally analyzed optically and electrically characterized as deposited and when annealed in argon for 1 hr in temperature range of 100 °C – 300 °C at interval of about 30 °C.

Results and Discussion

Transmittance, Reflectance and Absorbance. The as-deposited *In(OH)$_x$S$_y$* thin films were yellowish in colour but upon annealing in argon atmosphere for approximately 60 minutes they turned shiny and specular upon. The intensity of colour variation changed with annealing temperatures in the range of 100–300 °C. Those films annealed at 300 °C were the most specular. The average measured transmittance for the as grown *In(OH)$_x$S$_y$* thin films was 74.5 % in the wavelength range of 300-1100 m (Figure 2a) closer analysis revealed that such a high transmittance is theoretical equivalent to the optimum parameters for buffer layer applications in ETA-solar cells [18].

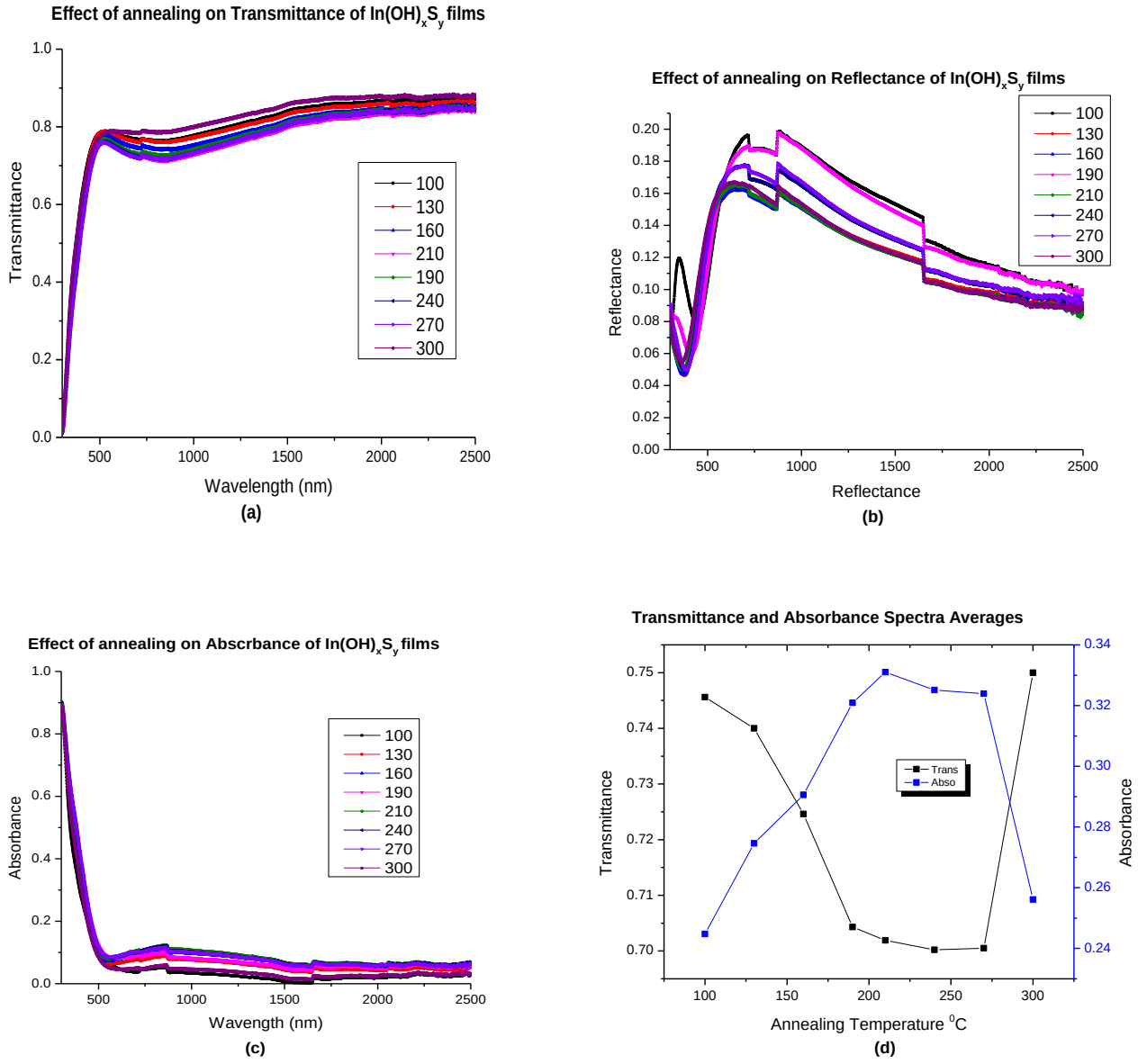

Figure 2 – Annealed curves for (a) Transmittance, (b) Reflectance, (c) Absorbance curves and (d) Comparison of transmittance and absorbance of *In(OH)$_x$S$_y$* thin films

A comparison was carried out for the annealed film and it was observed that (Figure 2d) an increase in annealing temperature up to 240 °C resulted into a slight decrease in transmittance which was followed by an increase as the annealing temperature was increasing. Thereafter, there was a sudden increase of transmittance. Such a behavior was attributed to material recrystallization [10] which caused a reduction of unsaturated defects alongside material decomposition. It was then explained that during thermal annealing [22], unsaturated defects gradually get annealed and the consequence is they produce large numbers of saturated bonds [17]. Such large saturated bonds in effect reduce the number of unsaturated defects [5] which in turn decreases the density of localized states in the band structure [22]. This finally result in increases the optical band gap [17, 5] best for light sensing and light absorption applications.

Band gaps. In curves demonstrating electronic band structure semiconductors, the band gap generally refers to the energy difference (in electron volts) between the top of the valence band and the bottom of the conduction band in insulators and semiconductors [20, 9]. In this work, energy band gap of the semiconductor $In(OH)_xS_y$ thin film was determined manually by extrapolating simulated data as depicted in Figure 3.

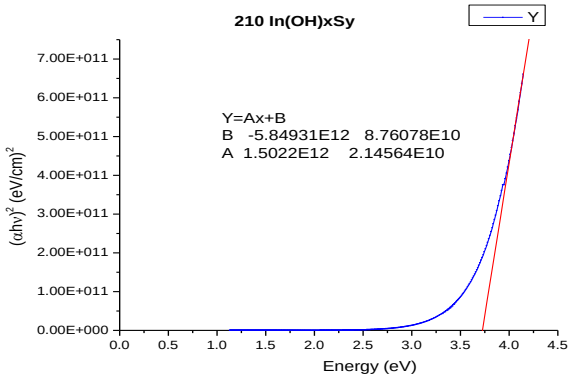

Figure 3 – Band gap of $In(OH)_xS_y$

By extrapolating the linear portions of the plots $(\propto h\nu)^2$ against $(h\nu)$ to where $(\propto h\nu)^2 = 0$, the value where the extrapolated line cuts energy $(h\nu)$ axis gives the thin film energy band gap. The results are given in the curve of figure 4. It was noted that the change in the energy band gap of $In(OH)_xS_y$ might be due to material recrystallization [10] and reduction of unsaturated defects during annealing [1]. These E_g values compare well with the literature values [1, 11, 20, 10, 17, 5, 22] that equally show that these were optimum values for solar cell applications [4, 17, 22].

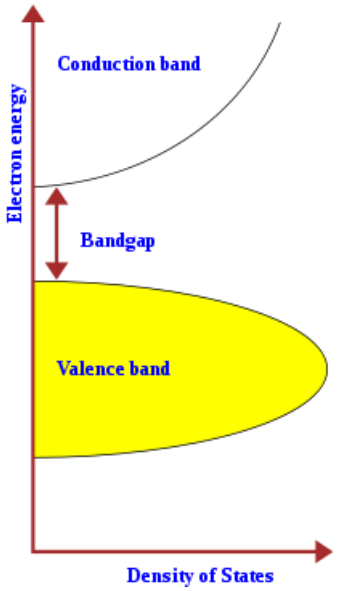

Figure 4 – Illustration of Band gap of $In(OH)_xS_y$ with density of states [9]

Energy band gap is usually referred to the energy difference between the conduction band and the valence band. The conduction band is the outermost energy band where the free electrons lie and below that there is the valence band [9]. An electron residing in the valence band cannot jump to the conduction band until and unless it is provided the amount of energy needed for the electron to cross the energy barrier between the aforementioned bands, which are just the band gap energy [4]. As soon as the electron is provided energy equal or greater than the band gap energy [5], it can go to the conduction band, become a free electron which is the main reason behind the high conductivity of metals. For an easy understanding, the raw experimental values obtained were tabulated in Table 1.

It can be observed that both the annealing temperature and the film thickness had major contributions to the experimental band gap obtained. Energy band gap is closely related to the HOMO/LUMO gap in chemistry [6]. If the valence band is completely full and the conduction band is completely empty, then electrons cannot move in the solid; however, if some electrons transfer from the valence to the conduction band, then current can flow. Therefore, the band gap is a major factor determining the electrical conductivity semiconductors [2, 9, 4].

Table 1: Band gaps of $In(OH)_xS_y$ films annealed in argon at different temperatures

Annealing temperature (°C)	Thin film thickness d (nm)	Energy Gap, E_g, (eV)
100	99.12 ± 0.28	3.73 ± 0.05
130	98.13 ± 0.27	3.68 ± 0.04
160	97.88 ± 0.26	3.53 ± 0.03
190	97.47 ± 0.26	3.51 ± 0.03
210	96.60 ± 0.26	3.51 ± 0.03
240	96.41 ± 0.26	3.49 ± 0.03
270	94.80 ± 0.26	3.67 ± 0.06
300	94.30 ± 0.20	3.72 ± 0.06

Usually the Band-gap energy of semiconductors tends to decrease with increasing temperature. This is attributed to atomic vibrations as temperature increases. When temperature increases as like when a thin film is being annealed, the amplitude of atomic vibrations increases. This leads to larger interatomic spacing becoming evident. As a consequence, the interaction between the lattice phonons and the free electrons and holes affect the band gap though to a smaller extent. As a result the relationship between band gap energy and temperature is the well described by *Varshni's* empirical expression (1):

$$E_g = E_{g(0)} - \frac{\alpha T^2}{T + \beta}, \quad (1)$$

where $E_{g(0)}$, α and β are material constants.

In a regular semiconductor crystal like that of $In(OH)_xS_y$ the band gap is fixed owing to continuous energy states[4]. But when analyzed at a quantum dot crystal level [20], the band gap is found to be size dependent and can be altered to produce a range of energies between the valence band and conduction band. Table 1 shows the errors estimation, but however, the error could also be due to quantum confinement effect [16] since band gaps also depend on pressure which was not investigated in this work. Equally, band gaps can be either direct or indirect, depending on the electronic band structure [25, 8] but in this work, the band gap was assumed to be direct [9].

Refractive index. The refractive index of a transparent optical medium, (index of refraction), is the factor by which the phase velocity V_{ph} is decreased relative to the velocity of light in vacuum [3], the refractive index also determines phenomena such as refraction, reflection and diffraction at optical interfaces (2):

$$V_{ph} = \frac{c}{\eta}. \quad (2)$$

The refractive index can be calculated from the relative permittivity ε and the relative permeability μ of a material (3):

$$\eta^2 = \varepsilon\mu. \quad (3)$$

The values of ε and μ at the optical frequency have to be used, which can deviate substantially from those at low frequencies. For usual optical materials, μ is close to unity. The values of refractive indices of $In(OH)_xS_y$ deduced from scout software by fitting of experimental data were in the range of 1.71–1.85 in the visible range that were appropriate for photovoltaic and solar cell applications. For $In(OH)_xS_y$ the refractive index, η, shows a general decrease as the wavelength increases for all the annealing temperatures. The refractive index of a material depends on the optical frequency or wavelength; this dependency is called chromatic dispersion [9]. Typical refractive index values for glasses used as substrates in the visible spectral region are in the range from 1.4 to 2.8 and therefore high transmission of materials, lies between spectral regions of strong absorbance [18]: the ultraviolet region with photon energies above the bandgap, and the near- or mid-infrared region with vibrational resonances [8] and their overtones. The refractive index is generally also dependent on the temperature of the material. In many cases, it rises with increasing temperature. In case of rare-earth-doped laser crystals [25, 10], the refractive index change caused by the doping is often quite small due to a low doping concentration.

Electrical Properties. Surface resistivity could be defined as the material's inherent surface resistance to current flow multiplied by that ratio of specimen surface dimensions (width of electrodes divided by the distance between electrodes) which transforms the measured resistance to that obtained if the electrodes had formed the opposite sides of a square [15]. In other words, it is a measure of the material's surface inherent resistance to current flow. Surface resistivity does not depend on the physical dimensions of the material. Ohm's law for circuit theory [16], the resistance of a material is the applied voltage divided by the current drawn across the material across two electrodes. Therefore, electrical resistance is proportional to the sample's length and the resistivity and inversely proportional to the samples cross sectional area (4):

$$R = \frac{V}{I} = \frac{\rho l}{A}, \quad (4)$$

where R – resistance of an object, Ω; V= Voltage, V; I – current through, A; ρ – electrical resistivity, Ω × m; A – cross-sectional area, m²; l – length of conductor, m.

The electrical resistivity of $In(OH)_xS_y$ films as measured by using the four point probe interfaced with the Keithley 2400 source meter is tabulated in Table 2.

Table 2 – Electrical resistivity and conductivity of $In(OH)_xS_y$ with annealing temperature

Annealing temperature (°C)	Thickness d (nm)	Resistivity ρ (Ωcm)	Conductivity σ (Ω-1cm-1)
100	99.12 ± 0.28	$9.03 \pm 0.35 \times 10^{7}$	$1.11 \pm 0.06 \times 10^{-8}$
130	98.13 ± 0.27	$9.00 \pm 0.34 \times 10^{7}$	$1.11 \pm 0.06 \times 10^{-8}$
160	97.88 ± 0.26	$8.90 \pm 0.34 \times 10^{7}$	$1.12 \pm 0.06 \times 10^{-8}$
190	97.47 ± 0.26	$8.82 \pm 0.33 \times 10^{7}$	$1.13 \pm 0.06 \times 10^{-8}$
210	96.60 ± 0.26	$8.76 \pm 0.32 \times 10^{7}$	$1.14 \pm 0.06 \times 10^{-8}$
240	96.41 ± 0.26	$8.72 \pm 0.31 \times 10^{7}$	$1.15 \pm 0.06 \times 10^{-8}$
270	95.80 ± 0.26	$1.01 \pm 0.51 \times 10^{8}$	$9.90 \pm 0.06 \times 10^{-9}$
300	94.30 ± 0.20	$1.02 \pm 0.51 \times 10^{8}$	$9.80 \pm 0.05 \times 10^{-9}$

As shown in Table 2 there was a slight decrease in electrical resistivity of the $In(OH)_xS_y$ thin films with increase in annealing temperature up to 240 °C when a significant increase in resistivity is realized appropriate for light emitting diodes [12], and photo detectors applications [25, 9]. The initial increase can be attributed to improved re-crystallization [10] of the crystal lattice of the $In(OH)_xS_y$ films before the increase of boundary scattering centers that may be was due to film decomposition that could have created vacancies resulting from evaporation of sulphur or elimination of hydroxyl group on further annealing.

Conclusions

$In(OH)_xS_y$ thin films were successfully prepared on glass substrates using CBD technique under different conditions and deposition parameters. The effect of annealing on optical and electrical properties of $In(OH)_xS_y$ was investigated and it was found out that the band gap energy values, E_g for as-deposited ranged between 2.79–3.32 eV. Transmittance decreased with sudden increases at about 270 °C that was attributed to re-crystallization since the films had large band gaps with low extinction and absorption coefficients. The electrical sheet resistivity was found to be $9.03 \pm 0.35 \times 10^{7}$ Ω × cm and the thin film characteristics obtained showed that the films could form good materials for optoelectronic applications especially in solar cells, light emitting diodes, and photo detectors.

Acknowledgement

The authors acknowledge the support give by the University of Nairobi for allowing access to the instruments used for characterization, Technical University of Mombasa and Kenyatta University and Maasai Mara University respectively.

References

1. Alonzo-Medina, G. M., González-González, A., Sacedón, J. L., & Oliva, A. I. (2013). Understanding the thermal annealing process on metallic thin films. *IOP Conference Series: Materials Science and Engineering, 45*, 1–6. doi: 10.1088/1757-899X/45/1/012013
2. Ao, Z., Song, G., & Xu, Y. (2017, January). Radiation characteristics of photoconductive antennas based on low-temperature grown GaAs. In *International Conference on Optoelectronics and Microelectronics Technology and Application*. doi: 10.1117/12.2264359
3. Chen, J., Ng, J., Lin, Z., & Chan, C. T. (2011). Optical pulling force. *Nature photonics, 5*, 531-534. doi: 10.1038/nphoton.2011.153
4. Ellis, B., Mayer, M. A., Shambat, G., Sarmiento, T., Harris, J., Haller, E. E., & Vučković, J. (2011). Ultralow-threshold electrically pumped quantum-dot photonic-crystal nanocavity laser. *Nature Photonics, 5*(5), 297–300. doi: 10.1038/nphoton.2011.51
5. Fan, R., Zhang, P., Shen, H., & Zhai, H. (2017). Out-of-time-order correlation for many-body localization. *Science Bulletin, 62*(10), 707–711. doi: 10.1016/j.scib.2017.04.011
6. Ito, S., Tanaka, S., Manabe, K., & Nishino, H. (2014). Effects of surface blocking layer of Sb_2S_3 on nanocrystalline TiO_2 for $CH_3NH_3PbI_3$ perovskite solar cells. *The Journal of Physical Chemistry C, 118*(30), 16995–17000. doi: 10.1021/jp500449z
7. Jiang, T., Huang, R., & Zhu, Y. (2014). Interfacial sliding and buckling of monolayer graphene on a stretchable substrate. *Advanced Functional Materials, 24*(3), 396–402. doi: 10.1002/adfm.201301999
8. Khorasani, A., Gibson, I., Goldberg, M., & Littlefair, G. (2017). On the role of different annealing heat treatments on mechanical properties and microstructure of selective laser melted and conventional wrought Ti-6Al-4V. *Rapid Prototyping Journal, 23*(2), 295–304. doi: 10.1108/RPJ-02-2016-0022
9. Lin, Y. H., Lin, S. F., Chi, Y. C., ... & Lin, G. R. (2015). Using n- and p-Type Bi_2Te_3 Topological Insulator Nanoparticles to Enable Controlled Femtosecond Mode-Locking of Fiber Lasers. *ACS Photonics, 2*(4), 481–490. doi: 10.1021/acsphotonics.5b00031
10. Liu, X., Sun, J., Yang, Y., Zhou, F., Pu, Z., Li, L., & Zheng, Y. (2016). Microstructure, mechanical properties, in vitro degradation behavior and hemocompatibility of novel Zn–Mg–Sr alloys as biodegradable metals. *Materials Letters, 162*, 242–245. doi: 10.1016/j.matlet.2015.07.151
11. Luangchaisri, C., Dumrongrattana, S., & Rakkwamsuk, P. (2012). Effect of heat treatment on electrical properties of fluorine doped tin dioxide films prepared by ultrasonic spray pyrolysis technique. *Procedia Engineering, 32*, 663–669. doi: 10.1016/j.proeng.2012.01.1324
12. Ly, K. T., Chen-Cheng, R. W., Lin, H. W., Shiau, Y. J., Liu, S. H., Chou, P. T., Tsao, C.-S., Huang Y.-C., & Chi, Y. (2017). Near-infrared organic light-emitting diodes with very high external quantum efficiency and radiance. *Nature Photonics, 11*, 63–68. doi: 10.1038/nphoton.2016.230
13. Mwathe, P., Musembi, R., Munji, M., Nyongesa, F., Odari, B., Njoroge, W., Aduda, B., & Muthoka, B. (2015). Effect of Annealing and Surface Passivation on Doped SnO2 Thin FilmsPrepared by Spray Pyrolysis Technique. *Advance in Materials, 4*(3), 51–58. doi: 10.11648/j.am.20150403.12
14. Opasanont, B., & Baxter, J. B. (2015). Dynamic Speciation Modeling to Guide Selection of Complexing Agents for Chemical Bath Deposition: Case Study for ZnS Thin Films. *Crystal Growth & Design, 15*(10), 4893–4900. doi: 10.1021/acs.cgd.5b00789
15. Rathmell, A. R., Bergin, S. M., Hua, Y. L., Li, Z. Y., & Wiley, B. J. (2010). The growth mechanism of copper nanowires and their properties in flexible, transparent conducting films. *Advanced materials, 22*(32), 3558–3563. doi: 10.1002/adma.201000775

16. Roetzel, W., Putra, N., & Das, S. K. (2003). Experiment and analysis for non-Fourier conduction in materials with non-homogeneous inner structure. *International Journal of Thermal Sciences, 42*(6), 541–552. doi: 10.1016/S1290-0729(03)00020-6

17. Swingle, B., & Chowdhury, D. (2017). Slow scrambling in disordered quantum systems. *Physical Review B, 95*. doi: 10.1103/PhysRevB.95.060201

18. Tsujimoto, K., Nguyen, D. C., Ito, S., ... & Tennakone, K. (2012). TiO_2 surface treatment effects by Mg^{2+}, Ba^{2+}, and Al^{3+} on Sb_2S_3 extremely thin absorber solar cells. *The Journal of Physical Chemistry C, 116*(25), 13465–13471. doi: 10.1021/jp208937j

19. Vliet, D. F., Wang, C., Tripkovic, D., ... & Stamenkovic, V. R. (2012). Mesostructured thin films as electrocatalysts with tunable composition and surface morphology. *Nature materials, 11*, 1051–1058. doi: 10.1038/nmat3457

20. Wang, P., Zhang, Y., Ruan, C., Su, L., Cui, H., & William, W. Y. (2017). A Few Key Technologies of Quantum Dot Light-Emitting Diodes for Display. *IEEE Journal of Selected Topics in Quantum Electronics, 23*(5), 1–12. doi: 10.1109/JSTQE.2017.2665779

21. Wei, J., Zang, Z., Zhang, Y., Wang, M., Du, J., & Tang, X. (2017). Enhanced performance of light-controlled conductive switching in hybrid cuprous oxide/reduced graphene oxide (Cu_2O/rGO) nanocomposites. *Optics Letters, 42*(5), 911–914. doi: 10.1364/OL.42.000911

22. You, Y. Z., Ludwig, A. W., & Xu, C. (2017). Sachdev-Ye-Kitaev model and thermalization on the boundary of many-body localized fermionic symmetry-protected topological states. *Physical Review B, 95*. doi: 10.1103/PhysRevB.95.115150

23. Yu, X., Pekker, D., & Clark, B. K. (2017). Finding Matrix Product State Representations of Highly Excited Eigenstates of Many-Body Localized Hamiltonians. *Physical Review Letters, 118*(1). doi: 10.1103/physrevlett.118.017201

24. Zhang, Q., Huang, Y., Xu, L., Cao, J. J., Ho, W., & Lee, S. C. (2016). Visible-Light-Active Plasmonic Ag–$SrTiO_3$ Nanocomposites for the Degradation of NO in Air with High Selectivity. *ACS Applied Materials & Interfaces, 8*(6), 4165–4174. doi: 10.1021/acsami.5b11887

25. Zhong, M., Hisatomi, T., Kuang, Y., ... & Domen, K. (2015). Surface Modification of CoO_x Loaded $BiVO_4$ Photoanodes with Ultrathin *p*-Type NiO Layers for Improved Solar Water Oxidation. *Journal of the American Chemical Society, 137*(15), 5053-5060. doi: 10.1021/jacs.5b00256